Table 9.3.2.1
Summary of various algorithms

The algorithms are, from top to bottom: error reduction, solvent flipping, hybrid input–output, difference map, averaged successive reflections, hybrid projection–reflection and relaxed averaged alternating reflections. A reflection is defined by its associated projection as $\mathbf{R} = 2\mathbf{P} - \mathbf{I}$, where $\mathbf{I}$ is the identity projection (Marchesini, 2007).

Algorithm	Iteration $\rho^{(n+1)} =$
ER	$\boldsymbol{P}_s\boldsymbol{P}_m\rho^{(n)}$
SF	$\boldsymbol{R}_s\boldsymbol{P}_m\rho^{(n)}$
HIO	$\begin{cases}\boldsymbol{P}_m\rho^{(n)}(\boldsymbol{r}), & \boldsymbol{r}\in S\\ (\boldsymbol{I}-\beta\boldsymbol{P}_m)\rho^{(n)}(\boldsymbol{r}), & \boldsymbol{r}\notin S\end{cases}$
DM	$\{\boldsymbol{I}+\beta\boldsymbol{P}_s[(1+\gamma_s)\boldsymbol{P}_m-\gamma_s\boldsymbol{I}] -\beta\boldsymbol{P}_m[(1+\gamma_m)\boldsymbol{P}_s-\gamma_m\boldsymbol{I}]\}\rho^{(n)}$
ASR	$(1/2)[\boldsymbol{R}_s\boldsymbol{R}_m+\boldsymbol{I}]\rho^{(n)}$
HPR	$(1/2)\{\boldsymbol{R}_s[\boldsymbol{R}_m+(\beta-1)\boldsymbol{P}_m]+\boldsymbol{I}+(1-\beta)\boldsymbol{P}_m\}\rho^{(n)}$
RAAR	$[(1/2)\beta(\boldsymbol{R}_s\boldsymbol{R}_m+\boldsymbol{I})+(1-\beta)\boldsymbol{P}_m]\rho^{(n)}$

been demonstrated in two dimensions, although the total efficiency of the optic used was of the order of 1% (Chao *et al.*, 2009) at the highest spatial frequencies. Thus, at the cost of throughput and ease of use, a diffraction microscope provides increased X-ray efficiency and resolution.

The following sections first report on the current standard single-particle phase retrieval techniques and then on recent experiments in CXDM, which establish the state of the art in whole-cell imaging by diffractive methods. Images of dry yeast at 11 nm resolution are presented, which represent the highest resolution X-ray images of whole cells currently on record. The effects of radiation damage are discussed and Sayre's idea of using stereoscopic viewing as a means of obtaining quick and low-dose three-dimensional information is explored (Sayre, 2008).

9.3.2. Phase retrieval from single-particle diffraction data

The problem of phase retrieval is solved through successive application of constraints on the recovered object in the data and object spaces. Using the language of convex optimization, the mathematical operators which act on the data are projectors. The projector in the reciprocal (data) space forces the Fourier components to have the correct magnitude, while in object space finite support is enforced. To calculate the Fourier magnitude projector, one first needs to propagate the object density, ρ, to the data space by a Fourier transform, then replace the estimated magnitudes $|\tilde{\rho}|$ with the measured ones, $I^{1/2}$, and finally propagate back to real space. Using these transforms one simplifies the calculation of the projection, which becomes an element-wise operation on each recovered Fourier component. The forward $\mathcal{F}$ and inverse $\mathcal{F}^{-1}$ transforms must be incorporated into the operator defined in real space $\mathbf{P}_m$,

$$\mathbf{P}_m = \mathcal{F}^{-1}\tilde{\mathbf{P}}_m\mathcal{F}, \tag{9.3.2.1}$$

where the measured Fourier magnitudes are enforced in Fourier space by $\tilde{\mathbf{P}}_m$. Using the Fourier basis, one simply replaces the estimated magnitudes $|\tilde{\rho}|$ with the measured ones $I^{1/2}$, $[\tilde{\mathbf{P}}_m\tilde{\rho}(\boldsymbol{k}) = I(\boldsymbol{k})^{1/2}\tilde{\rho}(\boldsymbol{k})/|\tilde{\rho}(\boldsymbol{k})|]$. Similarly, in the object space the finite support constraint is applied on a per pixel basis through multiplication by the support mask. The corresponding projector is

$$\mathbf{P}_s\rho = S\cdot\rho.$$

Table 9.3.2.1 lists the combination of projections used by the most popular algorithms.

The violation of the support constraint is used as an error metric to monitor the convergence towards the solution. The solution should have zero density outside the support mask, so the error can be defined as the total density outside the support area,

$$\varepsilon_s^2(\rho) = |||\rho - S\rho|||^2 = ||[I-\mathbf{P}_s]\rho||^2. \tag{9.3.2.2}$$

Alternatively, the error metric can be defined in the data space as the difference between the measured and calculated magnitudes,

$$\varepsilon_m^2(\rho) = |||\mathcal{F}\rho| - I^{1/2}||^2 = ||[I-\mathbf{P}_m]\rho||^2. \tag{9.3.2.3}$$

In reality, the measured intensities are subject to noise which prohibits exact compliance with the constraints, so the error metrics cannot drop to zero. Although in most cases the algorithm can locate the global minimum, random noise will force fluctuations around the minimum. Once the algorithm reaches this steady-state regime, any particular iterate chosen as the solution would have a misleading degree of detail. On the other hand, the average of many fluctuating iterates would have reduced intensity in those Fourier components which are not reliably phased. The ratio of the average Fourier magnitude to the measured magnitude provides a measure of the stability, or reproducibility, of the retrieved phase information. This ratio as a function of spatial frequency is the phase retrieval transfer function (PRTF),

$$\mathrm{PRTF}(\mathbf{q}) = \frac{|\mathcal{F}[\langle\psi\rangle]|(\mathbf{q})}{[I_m(\mathbf{q})]^{1/2}}, \tag{9.3.2.4}$$

where $\mathcal{F}[\langle\psi\rangle]$ is the Fourier transform of the final averaged image and I_m is the measured intensity pattern. The PRTF is analogous to the differential phase residual of electron microscopy and, following Chapman *et al.* (2006), the resolution of a reconstruction is chosen as the spatial frequency at which the PRTF falls below a value of 0.5.

9.3.3. High-resolution imaging of yeast

The X-ray dose required to image a given volume of protein is nearly independent of energy above the oxygen K edge. At the same time, the photon flux required to image the same volume increases with E^2 because of the energy dependence of the scattering cross section (Howells *et al.*, 2009). For this reason, it is advantageous to use the lowest energy commensurate with the desired resolution of 5–10 nm. Commercially available charge-coupled device (CCD) detectors can easily provide a scattering angle of 0.1 radians [a 1 inch detector placed 5 inches from the sample (1 inch = 2.54 cm)], which results in a half-period resolution of 8 nm when using 750 eV X-rays. Furthermore, a cell with a diameter of 3 µm would have an oversampling ratio (number of intensity samples per speckle) of at least ten in this geometry if the detector has 20 µm pixels.

In this particular case, a Princeton Instruments CCD (PI-MTE:1300) is placed 136 mm downstream of a freeze-dried yeast cell using the CXDM instrument on Beamline 9.0.1 of the Advanced Light Source (ALS). The yeast cell is illuminated by a coherent beam of 750 eV X-rays defined by a 5 µm pinhole located 25 mm upstream. The incident intensity of 4×10^6 photons s^{-1} μm^{-2} is high enough to cause rapid structural changes to the cell (discussed in the next section), so the sample requires pre-irradiation for about 30 minutes prior to collection of the final data set intended for reconstruction. The

final data set, shown in Fig. 9.3.3.1, is a 1024 × 1024 pixel subset of the full CCD and extends to a resolution of 11 nm at the edge and 7.8 nm in the corner. Speckles extend to the corner of the data set after a total exposure of 406 s and to the edge after 226 s.

The full reconstruction of this type of data set can only proceed once a high-fidelity support is determined. Algorithmic support determination using *Shrinkwrap*, a variation on the hybrid input–output algorithm, is straightforward for objects with sharp boundaries, as is often the case in the material sciences (Marchesini *et al.*, 2003; Chapman *et al.*, 2006). However, biological samples which often have soft boundaries require manual intervention in the early stages of reconstruction. The soft-edge problem is exacerbated by the loss of low spatial frequency information behind the beamstop. A combination of *Shrinkwrap* support adjustments and intuitively reasonable manual adjustments are made until the algorithm is stable to automatic adjustment. This point is found when further *Shrinkwrap* adjustments no longer alter the shape of the support but just its tightness. High-fidelity reconstructions of complex-valued objects are not possible with a loose support (Fienup, 1987). Once the support is found, the final image is produced as the average over many reconstructions, all using the same support, which are started from different random phase sets. This averaging procedure, discussed earlier, reduces features that are primarily due to noise and provides a measure of the reproducibility of the recovered phases and therefore an estimate of the resolution. The final reconstruction shown in Fig. 9.3.3.1 had PRTF values above 0.5 for spatial frequencies extending to the edge of the data set or 11 nm resolution. The inset image clearly shows features of the order of 15 nm in size. In general, it is not possible to identify cell organelles without labelling specific proteins. However, a correlative study of yeast which combines high-resolution CXDM with optical fluorescence would be a powerful tool for the cell-biology community. This technique has already been demonstrated at lower resolutions using a transmission X-ray microscope (Le Gros *et al.*, 2009).

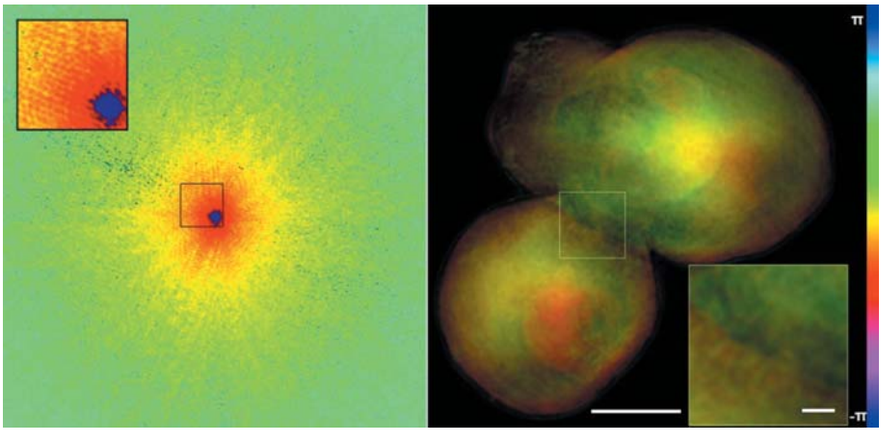

Figure 9.3.3.1
Diffraction pattern (left) and reconstruction (right) of a freeze-dried budding yeast cell. The diffraction pattern, measured on Beamline 9.0.1 of the ALS, extends to a half-period resolution of 11 nm and required 226 s of X-ray exposure. The blue regions of the diffraction pattern represent zeroes (noisy measurements or pixels lost behind the beamstop) and were left unconstrained during phase retrieval. The image represents the complex-valued X-ray wavefield after passing completely through the scattering potential, but propagated to the interior plane with the smallest support. The X-ray phase is represented as image hue and magnitude as brightness. The PRTF (not shown) never dips below 0.5, indicating that the magnitudes were adequately phased to the corner of the recorded data. The large scale bar is 1 μm, while the inset scale bar is 100 nm. The reconstruction presented here is the average of 25 independent reconstructions, each starting with a different set of random phases. Each reconstruction required 2000 iterations of the hybrid input–output algorithm and took about 14 s to complete on an nVidia Tesla C1060 graphics processing unit.

9.3.3.1. Radiation damage

High-resolution imaging of single particles with X-rays requires a large radiation dose because of the very strong dependence of the scattering cross section on spatial frequency and because, in the single-particle case, there is none of the coherent amplification one obtains when many identical copies of the particle are arranged into a crystal. This large dose means that either the sample must be protected from morphological changes induced by radiation exposure, most effectively through cryogenic techniques, or that the obtained images will represent an altered form of the original sample. Cryoprotection of hydrated cells has been successfully used in electron microscopy and lens-based X-ray microscopy for some time, but the sample preparation requirements of diffractive imaging are more severe, so the development of cryotechniques has been slower. The requirements of a finite sample support and that the sample be maintained on a zero-scattering background are extraordinarily difficult to achieve when that background consists of a micron-thick layer of ice. This is an active area of research by several X-ray diffraction microscopy groups.

For the case of dry cells, various preparation techniques (freeze drying or chemical fixation and dehydration) can preserve the large-scale internal structure, such as the size and shape of large organelles, but the ultrastructure will inevitably show artifacts of the drying process. Furthermore, exposure to ionizing radiation results in the well known shrinkage problem. Studies with a transmission X-ray microscope indicate that X-ray induced shrinkage primarily produces a higher-density but smaller version of the original cell (Jearanaikoon & Abraham-Peskir, 2005). The effect of cell shrinkage on the X-ray diffraction pattern is shown in Fig. 9.3.3.2. A freeze-dried cell is repeatedly exposed to 750 eV X-rays from Beamline 9.0.1 of the ALS. Each exposure is 30 s and delivers an X-ray dose of approximately 5×10^8 Gy. The sample is stable for the first two exposures but then experiences a rapid collapse, followed by a slow but continuous shrinkage. The collapse is apparent from the elongated speckles, which indicate a sample for which the diameter is changing during the exposure while its relative structure is maintained. Overall, the sample loses about 25% of its volume prior to the final exposure used for reconstruction (Shapiro *et al.*, 2005; Thibault *et al.*, 2006). Over the course of this exposure series the total scattered signal does not change, indicating that the total mass of the sample remains intact. The rapid change in the diffraction pattern during the early exposures means that successful imaging experiments require pre-irradiation of the sample. The slow but continuous shrinkage of dry samples with further dose means that the resolution of the three-dimensional images will necessarily be reduced. Indeed, Nishino *et al.* (2009) observed reduced resolution in their three-dimensional reconstruction of a dry

chromosome because of morphological changes which occurred during data collection. Hence, full three-dimensional imaging of cells by diffractive methods requires cryogenic protection against radiation damage. Predictions based on a calculation of the cross section for coherent scattering by a smooth dielectric indicate that 10 nm resolution imaging of frozen hydrated organic matter should be possible using soft X-rays at currently available synchrotron sources (Howells *et al.*, 2009). This limit is arrived at through a comparison of the radiation dose required for imaging and the dose at which radiation damage has been empirically observed at different length scales. However, it seems plausible that the presence of many identical particles within a cell could be exploited to provide super-resolution information.

9.3.3.2. Low-dose three-dimensional imaging; low damage potential of stereoscopic viewing

Diffraction imaging in three dimensions proceeds as it does in standard X-ray tomography. That is, two-dimensional data are recorded from many angular orientations of the sample and then assembled into a three-dimensional data set. In this case, however, the data are recorded in reciprocal space and the individual data sets only need to be registered with respect to the angular coordinate due to the Fourier shift theorem. In the absence of any additional information, the angular sampling of reciprocal space is determined by the Crowther resolution,

$$k_C = \frac{1}{\Delta\theta D},$$

where D is the object diameter and $\Delta\theta$ is the angular separation of the two-dimensional data sets. This is the spatial frequency at which the unmeasured Fourier components, those in between the measured Ewald sphere segments, can be properly interpolated from the measured data. Diffraction microscopy, however, requires the addition of information in the form of real-space constraints. This additional information allows for the calculation of not only the missing reciprocal-space phases but also a limited number of missing magnitudes. Chapman *et al.* (2006) showed that $\Delta\theta$ could in fact be up to four times larger than required by the Crowther relation, with k_C matching the numerical aperture of the imaging system. Thus, three-dimensional reconstructions could take place with nearly isotropic diffraction-limited resolution with only about 150 angular orientations of the sample.

Stereoscopic viewing can provide a significant degree of three-dimensional perception of an extended object while only increasing the total radiation exposure by a factor of two. In principle, according to the dose-fractionation theorem of Hegerl and Hoppe, full three-dimensional visualization of a given resolution element should not require a dose any higher than two-dimensional visualization of the same element with the same statistical accuracy (Hegerl & Hoppe, 1976). This theorem provides hope that high-resolution imaging in three-dimensions, perhaps even of dry specimens, is possible, but in practice this is very difficult to achieve and low-dose imaging techniques are only now being explored by the CXDM community. Stereoscopic viewing should be considered the preliminary low-dose technique of choice. One particular advantage is the rapid reconstruction (compared with full three-dimensional reconstructions) which makes possible *in situ* sample inspection. Fig. 9.3.3.3 shows a stereo image of a chemically dried budding yeast cell. When viewed stereoscopically, with the viewer's focus in front of the image, the three-dimensional arrangement of a group of vesicles in the mother cell can be visualized.

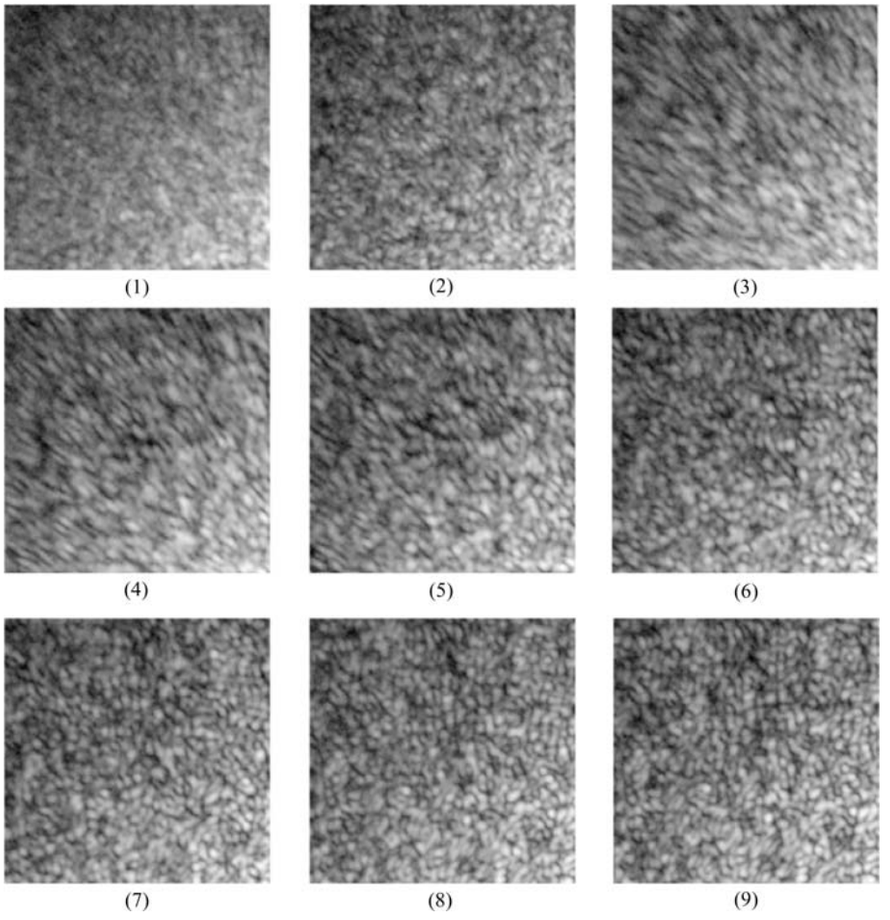

Figure 9.3.3.2
Exposure to ionizing radiation causes shrinkage of organic matter. Each image in this series is a section of a measured diffraction pattern from a freeze-dried yeast cell. The images were taken sequentially and each represents an additional X-ray dose of 5×10^8 Gy. After a cumulative dose of 1×10^9 Gy, the cell undergoes a rapid collapse [apparent from the elongated speckles in images (3)–(5)] followed by continued shrinkage at a reduced rate. The X-rays used had an energy of 750 eV and a dose of 5×10^8 Gy was adequate for reconstruction at 30 nm resolution. (Reproduced from Shapiro, 2004).

9.3.4. Conclusions

CXDM promises to be a highly efficient imaging methodology which can deliver high-resolution and high-contrast images of large non-crystalline biological structures. Radiation-induced shrinkage of dry cells will probably prohibit three-dimensional imaging of such cells at high resolution. However, significant three-dimensionality can be achieved through stereoscopic viewing of a cell, which only doubles the necessary X-ray dose. Even so, in the absence of low-dose diffraction techniques the sample must undergo considerable morphological change prior

references